







Predicting ductility in quaternary $B2$ -like alloys

Emily Hwang ^{1,*} Emma Cuddy ¹ Julianne Lin,¹ Jonas L. Kaufman ² Adam Shaw ³ Patrick L. J. Conway,⁴
Aurora Pribram-Jones,⁵ Kevin J. Laws ⁴ and Lori Bassman ¹

¹Harvey Mudd College, Claremont, California 91711, USA

²Materials Department, University of California, Santa Barbara, California 93106, USA

³Division of Physics, Mathematics, and Astronomy, California Institute of Technology, Pasadena, California 91125, USA

⁴School of Materials Science and Engineering, University of New South Wales (UNSW Sydney), Sydney 2052, Australia

⁵Department of Chemistry and Chemical Biology, University of California, Merced, California 95343, USA



(Received 1 October 2020; accepted 1 February 2021; published 11 March 2021)

Although intermetallics with a $B2$ -type crystal structure are typically brittle, a class of $B2$ intermetallics that demonstrates unusually high ductility has been reported. A set of recently developed $B2$ -like quaternary precious metal-rare earth alloys also includes compositions with significant ductility. To predict ductility in these systems, we have adapted a computational energy-based metric based on slip systems and relative stability of planar defects, developed to predict ductility in $B2$ binary systems, for use with quaternary $B2$ -like alloys. The computational metric successfully predicts the experimentally-determined ductility or brittleness of 15 $B2$ -like quaternary precious metal-rare earth and refractory alloys.

DOI: [10.1103/PhysRevMaterials.5.033604](https://doi.org/10.1103/PhysRevMaterials.5.033604)

I. INTRODUCTION

Intermetallic compounds with the CsCl $B2$ -type crystal structure are typically brittle. However, in 2003 Gschneidner *et al.* [1] found that a subset of the approximately 150 binary compounds with this structure show significant ductility. Subsequent study added to this list, with a summary of ductile $B2$ alloys presented by Gschneidner *et al.* in 2009 [2]. The significant differences in ductility among alloys with the same $B2$ crystal structure can be explained by the mobilities of the different types of dislocations that are favorably activated [3].

Inspired by these results, a set of multicomponent equiatomic alloys that exhibit preferred $B2$ -like site occupation of precious metal and rare earth constituents were created [4]. This set includes the first reported ductile equiatomic quaternary alloys with this crystal structure as well as brittle alloys with similar elemental constituents. These alloys present an opportunity to develop and experimentally validate a computational metric for ductility in quaternary $B2$ -like alloys.

Ductility in crystalline metals results from atoms gliding past one another via dislocation mechanisms where atomic bonds are stretched, rotated, and broken in a periodic manner to accommodate strain [5]. This process is also directly linked to the shear and bulk modulus of a material. From an electronic bonding perspective, this process is relatively easy if the core charges of the metal ions are identical and uniformly distributed, as in the case with a pure metal, allowing atoms to overcome a low-energy barrier and glide or shear past one another. However, in the case of multicomponent intermetallic compounds, complex intraelectron orbital bonding states

(hybridization) between dissimilar constituents typically occur. This often results in considerably stronger, more directional (covalent) bonding between atoms and charge localization within the crystal lattice [1,2]. As the number of electrons involved in a hybridized bond increases, the strength and stiffness of this bond increases with rising angular momentum quantum number. In the case of the p , d , and f bands, bonding is highly directional. Therefore when atoms of different ion-core charges in a multicomponent intermetallic compound glide past one another during shear, the energy required is much higher than for atoms with identical ion-core charges and the bonding character is often anisotropic [1,2]. If this energy barrier cannot be overcome for a sufficient number of slip systems, the material will be intrinsically brittle [5].

Established methods have exploited these physical characteristics of ductility to computationally predict ductility in $B2$ alloys. One method is to calculate the ratio of bulk to shear modulus, which can be used to establish a minimum cutoff value for ductility as shown by Wu and Hu [6]. However, this method has been found to have some limitations, as a cutoff value generally holds true only within a family of intermetallics. The cutoff presented by Wu and Hu is valid for binary $B2$ magnesium-rare earth intermetallics; however, applying that same value to the scandium-transition metal and copper-rare earth families incorrectly predicts the ductility of one third of the alloys and no other single value is more suitable. Therefore, a cutoff or explicit limit for the ratio of bulk to shear modulus is not accurate in predicting ductility for a wide range of alloys with limited prior experimental knowledge.

Methods based on investigating the bonding nature between constituents in $B2$ -structured compounds can also be used to predict ductility. With the density of states (DOS), the orbital occupancy near the Fermi energy can be used as an

*eyhwang@g.hmc.edu

indication of ductility, as *d*-orbital DOS peaks close to the Fermi energy implies that the bonding character will be more directional [7]. The electron localization function [8,9] and bonding charge distribution have been used to visualize the directionality of an alloy's bonding character. However, bonding nature alone in a static *B2* lattice can be too qualitative to reliably predict ductility as this relies on visual indicators to distinguish brittle from ductile materials. Although these literature methods have shown moderate success, an ideal computational metric of ductility should be applicable across alloy families, quantitative, and based on the underlying mechanisms of plastic deformation.

The *B2* crystal structure has two dominant slip systems, $\langle 111 \rangle \{1\bar{1}0\}$ and $\langle 111 \rangle \{11\bar{2}\}$, and two main slip directions, $\langle 111 \rangle$ and $\langle 001 \rangle$ [10,11]. Slip in the $\langle 111 \rangle$ direction has been linked with brittleness while $\langle 001 \rangle$ slip has potential for ductility [12]. Thus, favorable slip on the $\langle 111 \rangle \{1\bar{1}0\}$ system is associated with ductility due to the possibility of secondary dislocation motion in the $\langle 001 \rangle$ direction.

The two slip systems and the ductility associated with $\langle 001 \rangle$ slip result in two criteria for ductility in *B2* materials: $\langle 001 \rangle$ slip must be the dominant slip direction and multiple slip in the $\langle 111 \rangle$ direction should be possible. Sun and Johnson [13] implement these two criteria to create a quantitative metric for *B2* ductility. Their metric uses antiphase boundaries (APBs) and stacking faults (SFs) in the two slip systems, specifically the $\langle 111 \rangle \{1\bar{1}0\}$ APB, $\langle 001 \rangle \{1\bar{1}0\}$ SF, and $\langle 111 \rangle \{11\bar{2}\}$ APB (denoted here as APB $\{1\bar{1}0\}$, SF $\{1\bar{1}0\}$, and APB $\{11\bar{2}\}$, respectively). The planar defect energies, elastic constants, and lattice parameter are used to construct the following dimensionless quantities:

$$C = \frac{\gamma_{\text{APB}}^{\{1\bar{1}0\}}}{c_{44}a} \quad (1)$$

$$\delta = \frac{\gamma_{\text{SF}}^{\{1\bar{1}0\}}}{\gamma_{\text{APB}}^{\{1\bar{1}0\}}} \quad (2)$$

$$\lambda = \frac{\gamma_{\text{APB}}^{\{11\bar{2}\}}}{\gamma_{\text{APB}}^{\{1\bar{1}0\}}}, \quad (3)$$

where c_{44} is the isotropic shear modulus, a is the lattice parameter, and γ is the planar defect energy, given by

$$\gamma = \frac{E_{\text{defect}} - E_{\text{perfect}}}{mA}, \quad (4)$$

where E_{defect} is the total energy of the structure with planar defects, E_{perfect} is the total energy of the perfect structure, m is the number of defect planes in the structure, and A is the area of the defect plane.

Using these quantities and the slip system criteria, Sun and Johnson introduce two necessary conditions and one sufficient condition to predict ductility in *B2* systems. Full derivations of the necessary and sufficient conditions can be found in Ref. [13]. The necessary conditions address the favorability of APBs and SFs in the $\{1\bar{1}0\}$ plane. The first criterion, that $\langle 001 \rangle$ slip is more favorable than $\langle 111 \rangle \{1\bar{1}0\}$ slip. This yields the first necessary condition:

$$\ln C \geq \ln\left(\frac{3}{8\pi e}\right) - \ln\left(\frac{r_0}{a}\right) \approx -3.9, \quad (5)$$

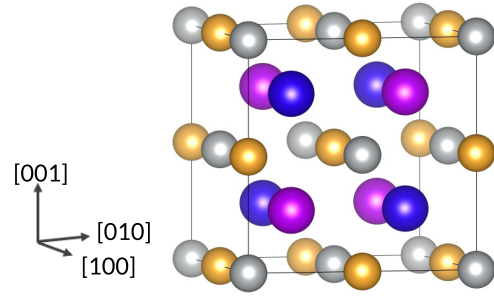


FIG. 1. The ordered quaternary *B2*-like unit cell. Each color represents a different element. For example, in the precious metal-rare earth quaternary alloys, gold and silver represent positions of the precious metal atoms while blue and pink represent the positions of the rare earth atoms. Structure images created using VESTA [18].

where e is Euler's number and r_0 is the dislocation core radius. A value of $2.5b$, where b is the magnitude of the Burgers vector, was chosen for the dislocation core radius to produce the numerical value of -3.9 in the inequality. Furthermore, to fulfill both criteria, APBs must be more energetically favorable than SFs. This results in the second necessary condition:

$$\ln \delta > -2.132 - \frac{1}{4} \ln C \quad (6)$$

where, similarly to Eq. (5), the first term on the right-hand side of the equation is a function of $\frac{r_0}{a}$, and substituting $2.5b$ for r_0 results in the numerical value of -2.132 .

The sufficient condition deals with the formation of APBs on both slip systems. In order for the second criteria, or multiple slip, to occur, APBs must be bistable on both the $\langle 111 \rangle \{1\bar{1}0\}$ and $\langle 111 \rangle \{11\bar{2}\}$ slip systems, producing the condition:

$$\frac{\sqrt{3}}{2} \leq \lambda \leq \frac{2}{\sqrt{3}}. \quad (7)$$

Together, the necessary and sufficient conditions can be used to construct stability maps to predict ductility. For a material to be predicted ductile, it must fulfill all three conditions.

Sun and Johnson use 23 binary *B2* alloys to test their method [13]. These alloys include ionic compounds, classic *B2* alloys, and a series of Y- and Sc-based compounds, many containing precious metals. The total ductility prediction has a 83% accuracy across the entire range of test alloys, demonstrating the promise of this metric. Of the compounds tested, AuZn, YIn, YRh, and ScRh are all incorrectly predicted to be brittle, though AuZn and YIn are noted to have either experimentally uncertain ordering or structure.

The set of *B2* materials investigated by Sun and Johnson include rare earth elements with the Y- and Sc-containing intermetallics, but they lack compounds that contain lanthanide metals. Since the ductile quaternary alloys of interest include elements from the lanthanide series, in this study we have validated Sun and Johnson's ductility metric for 10 binary lanthanide *B2* alloys and have confirmed their results for a set of 13 transition metal intermetallics. The ductility metric has also been extended to quaternary *B2*-like alloys (Fig. 1). The 11 quaternary alloys composed of precious metal (Ag, Au, Cu, Pd) and rare earth (Dy, Gd, Sc, Y) elements that were

confirmed to be single phase by x-ray diffraction and scanning electron microscopy have been investigated with the metric [4]. The four single-phase quaternary B2 refractory alloys reported in the review of refractory high entropy superalloys by Miracle *et al.* have also been explored with the metric to diversify the range of alloys studied [14–17]. The metric has proven to be less accurate for the quaternary alloys, so to extend its applicability, we propose a modification to their computational method by switching to a different functional approximation. With this modification, the computational predictions from the metric match the experimentally-determined ductility or brittleness of all 15 quaternary alloys.

II. METHODS

This work used density functional theory implemented in the Vienna *ab initio* simulation package (VASP) [19,20]. Projector augmented wave (PAW) potentials were used with both the Perdew-Burke-Ernzerhof (PBE) [21] and revised Perdew-Burke-Ernzerhof generalized gradient (PBEsol) [22] exchange correlation approximations. The electronic convergence algorithm chosen was the mixture of the blocked Davidson and RMM-DIIS algorithms (ALGO = Fast), recommended for systems with more than 20 atoms. Ionic relaxations used automatic real-space projections, and total energies were converged within 10^{-4} eV/cell. To obtain accurate final energies, each relaxation was followed by a static calculation with real-space projections turned off and with the tetrahedron method [23]. All calculations were non-spin-polarized and were performed with a plane wave energy cutoff of 450 eV.

The lattice parameter and elastic constants were obtained by applying lattice deformations to a two-atom unit cell for the binary alloys and a 16-atom unit cell for the quaternary alloys. The bulk modulus and lattice parameters were calculated by isotropically compressing the unit cell and fitting the resulting energy-volume data to the Birch-Murnaghan equation of state. The shear modulus c_{44} was determined by applying volume-conserving monoclinic deformations to the unit cell, then fitting to a known energy-volume relationship following Zaddach *et al.* [24].

For binary systems, the APB{ $1\bar{1}0$ } and SF{ $1\bar{1}0$ } planar defect energies were calculated with 32-atom structures [Fig. 2(a)] and a $16 \times 12 \times 1$ Γ -centered k -point mesh. The APB{ $11\bar{2}$ } defect energy was calculated with a 24-atom structure [Fig. 2(b)] and $13 \times 10 \times 4$ Γ -centered k -point mesh. Each cell included two faults; the { $1\bar{1}0$ } faults were separated by eight planes of atoms while the { $11\bar{2}$ } faults were separated by six planes of atoms. For each binary system, a two-atom unit cell was allowed to relax with a fixed equilibrium volume calculated from a Birch-Murnaghan fit as well as a fixed cell shape. The relaxed structure was tiled to the { $1\bar{1}0$ } and { $11\bar{2}$ } supercells and the appropriate faults were inserted (Fig. 2). Each perfect supercell was run as a static calculation before faults were added. For the faulted structures, two layers of atoms on either side of each fault were allowed to relax in the direction perpendicular to the fault, with the cell shape and volume fixed, followed by a static calculation.

For quaternary systems, the APB{ $1\bar{1}0$ } and SF{ $1\bar{1}0$ } planar defect energies were calculated with 128-atom structures

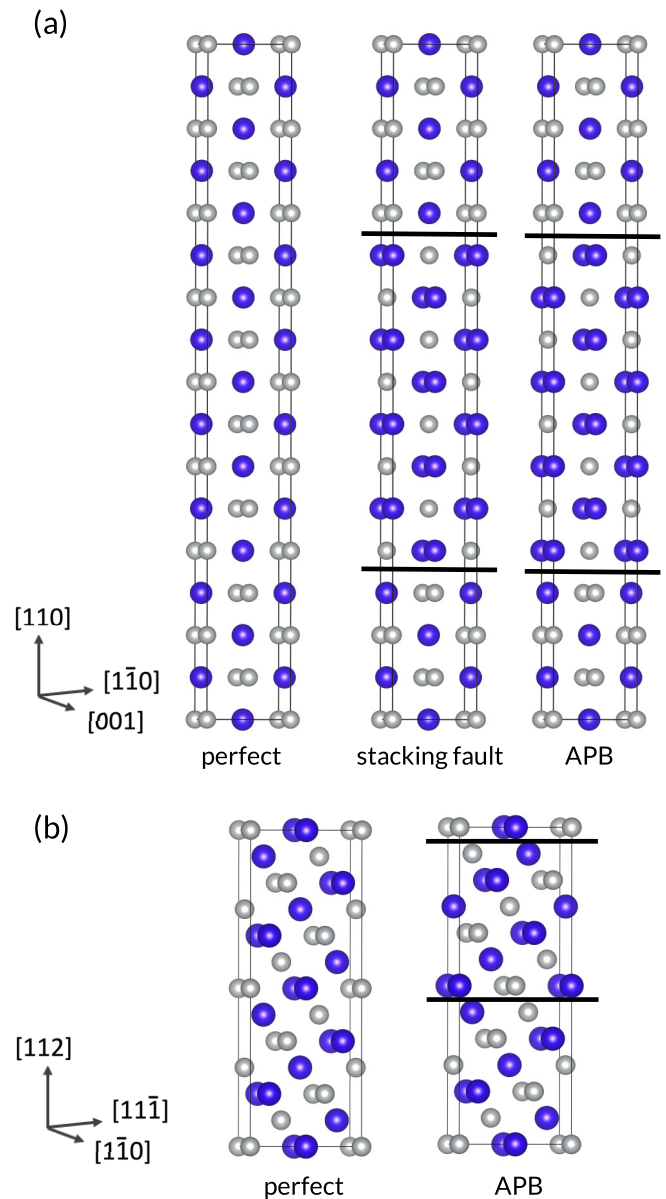


FIG. 2. The binary perfect and faulted structures used for determining the (a) stacking fault and antiphase boundary energies for the { $1\bar{1}0$ } plane and (b) antiphase boundary energy for the { $11\bar{2}$ } plane. Horizontal lines indicate locations of antiphase boundaries or stacking faults.

[Fig. 3(a)] and a $4 \times 4 \times 1$ Γ -centered k -point mesh. The APB{ $11\bar{2}$ } defect energy was calculated with a 96-atom structure [Fig. 3(b)] and $3 \times 3 \times 2$ Γ -centered k -point mesh. The number of faults and layers between the faults were consistent with the binary systems. The planar defect energies of the quaternary alloys were calculated in the same manner as the binary alloys with a 16-atom unit cell for the base structure rather than the two-atom binary cell. Deformation on the specified slip planes will periodically disorder and reorder the supercell structure of the quaternary alloys. The stacking fault configuration shown in Fig. 3 corresponds to the upper limit of the energy barrier needed to translate the dislocation. This

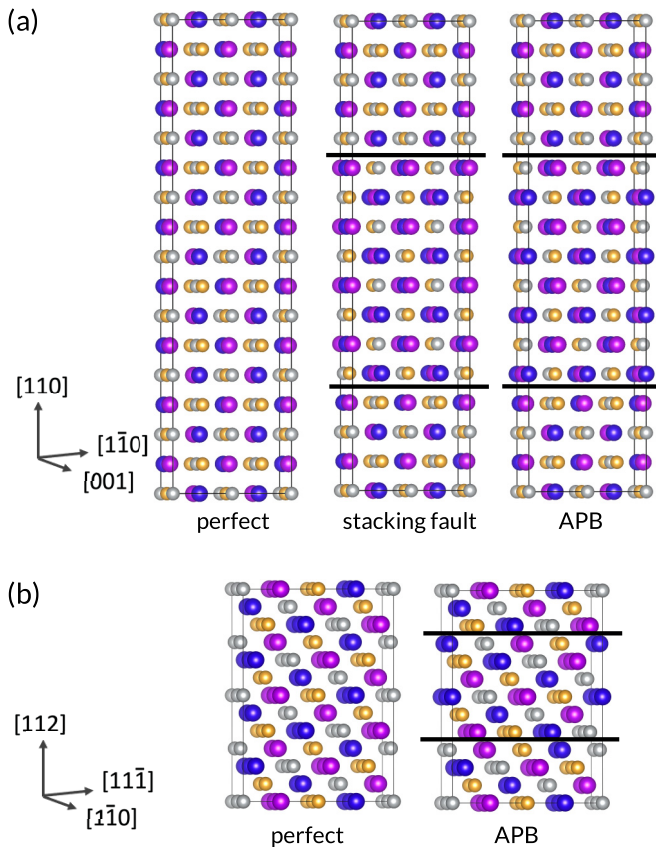


FIG. 3. The quaternary perfect and faulted structures used for determining the (a) stacking fault and antiphase boundary energies for the $\{1\bar{1}0\}$ plane and (b) antiphase boundary energy for the $\{11\bar{2}\}$ plane. Horizontal lines indicate locations of antiphase boundaries or stacking faults.

highest-energy stacking fault structure has been used with the ductility metric.

Note that for the quaternary alloys, alternate versions of the faulted structures could be considered through deformations by the $\langle 111 \rangle$ and $\langle \bar{1}\bar{1}\bar{1} \rangle$ shear vectors for antiphase boundaries and the $\langle 001 \rangle$ and $\langle 00\bar{1} \rangle$ for stacking faults. These pairs of shear vectors could create inequivalent faulted structures due to the lack of an inversion center in the quaternary structure. However, the atomic arrangements of the two defect planes within a single structure are different from each other, and when the direction of the shear vector is reversed, the two arrangements trade positions. Defect energy calculations for several alloys demonstrated that the fault energies are unchanged with this change in the shear vector. Therefore, the ductility metric can be implemented using one version of each faulted structure.

III. RESULTS AND DISCUSSION

The ductility metric has been evaluated for 12 binary $B2$ intermetallics to compare with Sun and Johnson's previous use of the metric as well as for an additional 10 binary intermetallics with a lanthanide component. Fifteen confirmed single-phase $B2$ -like quaternary alloys are also examined to extend the metric for quaternary systems. Of these 15 alloys,

11 are composed of precious metals and rare earth elements while the remaining four are composed of refractory metals. Although the metric demonstrates moderate success with the binary alloys on par with Sun and Johnson's results, it successfully predicts the ductility of all 15 quaternary alloys with a modification of the method by changing the PBE functional approximation to the PBEsol functional approximation.

A. Binary systems

The binary $B2$ metric from Sun and Johnson has been tested on a set of 22 $B2$ alloys. Results are shown in Fig. 4. These 22 alloys include 12 transition metal alloys already examined by Sun and Johnson, and ductility predictions for all alloys in this set match their results. Within this subset, the metric has a 83% accuracy rate, with incorrect predictions for YIn and AuZn. Both alloys are experimentally ductile but computationally brittle, and YIn fails the sufficient condition while AuZn fails both the necessary and sufficient conditions. AuZn and YIn additionally have some uncertainty within experimental data [1,7]. These two intermetallics are similarly mischaracterized in Sun and Johnson's results and have been intentionally included here to confirm that the mischaracterizations would be reproduced and to determine whether any modifications made to the method would improve the results. Given that the quaternary $B2$ -like alloys of interest contain lanthanide-group metals, an additional 10 binary $B2$ alloys with a lanthanide component have been tested with the ductility metric. For these alloys, the accuracy of the metric is 70%, with incorrect predictions for CuDy, CuGd, and CuHo. All three alloys are experimentally ductile but computationally predicted brittle; CuDy and CuGd both fail the sufficient condition while CuHo fails both the necessary and sufficient conditions. However, it is known that CuGd undergoes a martensitic transformation at 250 K from the $B2$ phase at higher temperatures to the $B27$ phase at lower temperatures, attributed to a $5d$ -band Jahn-Teller effect [25,26]. CuDy and CuHo are expected to undergo similar transformations. Therefore, the metric's mischaracterization of these alloys may result from the method constraining these alloys to the $B2$ structure at 0 K. Numerical values for the relevant metric quantities ($\ln C$, $\ln \delta$, λ) as well as mechanical properties and defect energies can be found in the Supplemental Material (Ref. [27]).

All calculations were repeated with the PBEsol functional to explore how the selection of functional approximation affects the results of the metric. While minor shifts are observed in the results, the overall ductility predictions of the binary alloys do not change with the incorporation of the PBEsol functional approximation. Of all 22 binary alloys, a substantial shift occurs only in YMg, which switches from fulfilling the sufficient condition and failing the necessary condition with PBE to failing the sufficient condition and residing on the cutoff of Eq. (6) with PBEsol. However, with either functional approximation, YMg is predicted to be brittle, so this shift does not change the overall ductility prediction of YMg.

B. Quaternary systems

The ductility metric has been applied to 15 quaternary alloys that have been confirmed to be single phase with a

| | PBE | | | PBEsol | | |
|------|---------------------|----------------------|--------------------|---------------------|----------------------|--------------------|
| | Necessary condition | Sufficient condition | Overall prediction | Necessary condition | Sufficient condition | Overall prediction |
| AuZn | N | N | ✗ | N | N | ✗ |
| FeAl | N | N | ✗ | N | N | ✗ |
| NiAl | Y | N | ✗ | Y | N | ✗ |
| ScAg | Y | Y | ✓ | Y | Y | ✓ |
| ScAu | Y | Y | ✓ | Y | Y | ✓ |
| ScCu | Y | Y | ✓ | Y | Y | ✓ |
| ScPd | Y | Y | ✓ | Y | Y | ✓ |
| ScRu | N | N | ✗ | N | N | ✗ |
| YAg | Y | Y | ✓ | Y | Y | ✓ |
| YIn | Y | N | ✗ | Y | N | ✗ |
| YMg | N | Y | ✗ | (N) | N | ✗ |
| YZn | Y | N | ✗ | Y | N | ✗ |
| AgLa | Y | Y | ✓ | Y | Y | ✓ |
| CuDy | Y | N | ✗ | Y | N | ✗ |
| CuGd | Y | N | ✗ | Y | N | ✗ |
| CuHo | N | N | ✗ | N | N | ✗ |
| MgCe | N | N | ✗ | N | N | ✗ |
| MgGd | N | Y | ✗ | N | Y | ✗ |
| MgHo | N | N | ✗ | N | N | ✗ |
| MgPr | N | N | ✗ | N | N | ✗ |
| ZnDy | Y | N | ✗ | Y | N | ✗ |
| ZnTb | Y | N | ✗ | Y | N | ✗ |

| | |
|-----------------------------------|---|
| experimentally brittle | ✗ |
| experimentally ductile | ✓ |
| computationally predicted brittle | ✗ |
| computationally predicted ductile | ✓ |

FIG. 4. Summary of the experimental and predicted computational ductility results for binary alloys calculated with the PBE and PBEsol functional approximations. The thick horizontal line between YZn and AgLa separates the transition metal intermetallics (above line) from intermetallics with a lanthanide component (below line). Y means that the alloy fulfilled that condition while N means that the alloy failed that condition. (N) signifies that the alloy is on the boundary of the condition.

B2-like crystal structure at room temperature. Eleven of these alloys are composed of precious metals and rare earth elements and the remaining four are refractory alloys reported in the literature [14]. The necessary conditions [Eqs. (5) and (6)] are visualized in a stability map by plotting $\ln \delta$ against

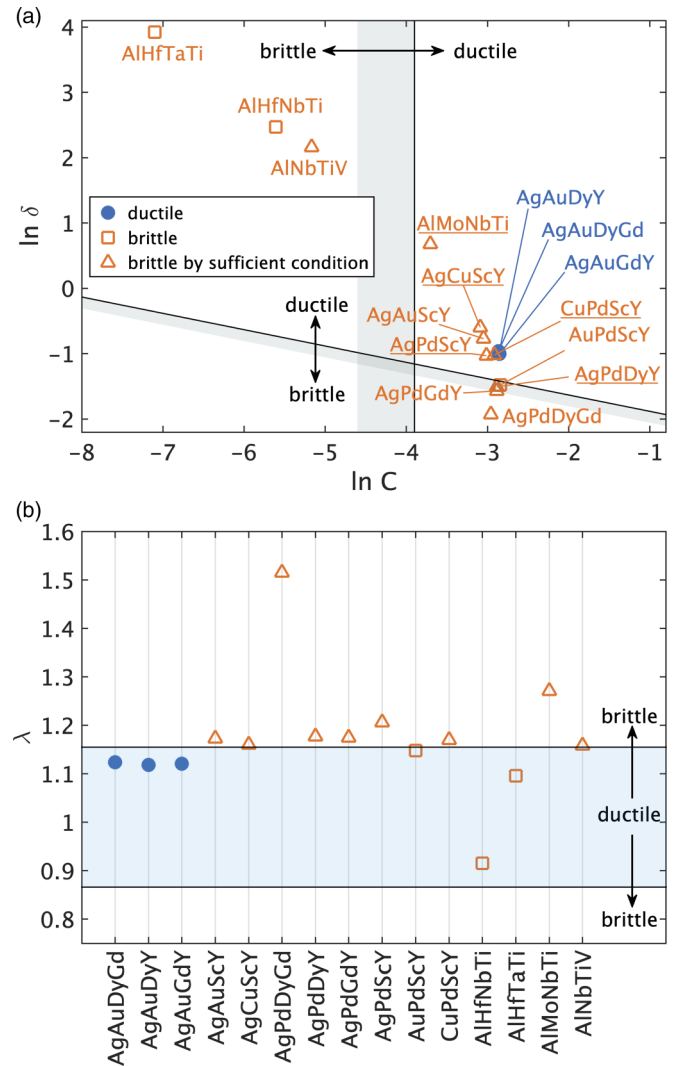


FIG. 5. Quaternary alloy results with the PBEsol functional approximation for the (a) necessary conditions and (b) sufficient condition. To be predicted as ductile, alloys must fall in the upper right region of (a) to satisfy the necessary conditions and within the blue shaded region of (b) to satisfy the sufficient condition. In (a), alloys that are predicted brittle due only to failing the sufficient condition are indicated with underlines. The gray shaded bands in (a) are discussed in the text and the solid lines separating the ductile and brittle regions mark the original necessary conditions from Ref. [13].

$\ln C$, shown in Fig. 5(a), while the sufficient condition [Eq. (7)] is shown by the value of λ in Fig. 5(b). In Fig. 5(a), the alloys that are predicted brittle only from failing the sufficient condition have labels marked with underlines. Alloys that fall in both the upper-right region of Fig. 5(a) and within the shaded region of Fig. 5(b) satisfy all conditions and are predicted ductile. All calculations were run with both the PBE and PBEsol functional approximations and with structures appropriately modified for the quaternary alloys (Fig. 3). The ductility metric successfully predicts 11 out of the 15 quaternary B2-like alloys with PBE, but the metric successfully predicts all 15 of the quaternary alloys with PBEsol.

The necessary conditions in Sun and Johnson’s method have one free parameter, the dislocation core radius (r_0),

which has an accepted range of b to $5b$ for edge dislocations [5]. Work from Xu and Moriarty [28] shows that $2b$ is a good approximation for the radius in pure body-centered cubic (bcc) Mo. Sun and Johnson then assume that the radius should be larger for binary systems than for pure metals and state that a reasonable range of values for binary $B2$ systems is $2.5b$ to $5b$. The necessary conditions [Eqs. (5) and (6)] are then derived using the lower end of this range ($2.5b$). However, the whole range can be explored by using both values as limiting cases. Replacing the dislocation core radius with the value of $5b$ results in the following lower bounds for the necessary conditions:

$$\ln C \geq -4.6 \quad (8)$$

$$\ln \delta > -2.305 - \frac{1}{4} \ln C \quad (9)$$

Thus for quaternary alloys, gray shaded bands are used to show the range of possible locations of the necessary condition boundaries in Fig. 5(a). In the same figure, the solid lines separating the ductile and brittle regions mark the original necessary conditions [Eqs. (5) and (6)] with the dislocation core radius of $2.5b$. None of the quaternary alloys fall in the vertical band that results from Eqs. (5) and (8) while three alloys (AuPdScY, AgPdDyY, AgPdGdY) are located in the sloped band that results from Eqs. (6) and (9), noted as N* in Fig. 6. Of these three alloys, AgPdDyY and AgPdGdY are correctly predicted brittle based on the sufficient condition while AuPdScY does not fail the sufficient condition. Because AuPdScY is experimentally brittle, using the lower boundary would result in an incorrect prediction. Although the bands allow for the exploration of the whole range of values of the dislocation core radius, changing the necessary conditions did not improve correspondence with experimental results. Therefore, the original cutoff [Eqs. (5) and (6)] is recommended for future use.

Several alloys (AgPdDyGd, AgPdDyY, AgPdGdY) are noted in Fig. 6 to be marginally ductile from experiment and are predicted brittle with the quaternary ductility metric. The designation of marginal ductility comes from qualitative observations while cutting samples and quantitative hardness data that distinctly separates the alloys: The average hardness (\pm standard deviation) of the ductile alloys is 162 ± 11 HV, the average hardness of the marginally ductile alloys is 232 ± 14 HV, and the average hardness of the brittle alloys is 385 ± 11 HV (individual values in Supplemental Material [27]). Here hardness tends to correspond to qualitative ductility: The low hardness alloys demonstrate substantial ductility as confirmed by compression tests [4]; the intermediate hardness alloys show some signs of bending ductility at the final stages of cutting with a diamond saw blade but are not sufficiently ductile to fabricate compression test samples, and the high hardness alloys demonstrate clear brittleness. Prediction of the marginally ductile alloys as brittle indicates that the metric predicts alloys as brittle unless the composition demonstrates substantial ductility.

For the sufficient condition [Eq. (7)], Y. Sun [11] presents results as a stability map of λ against another dimensionless parameter based on the elastic constants. This plot can help elucidate the dominant slip system. However, to determine

| | PBE | | | PBEsol | | |
|----------|---------------------|----------------------|--------------------|---------------------|----------------------|--------------------|
| | Necessary condition | Sufficient condition | Overall prediction | Necessary condition | Sufficient condition | Overall prediction |
| AgAuDyGd | Y | Y | ✓ | Y | Y | ✓ |
| AgAuDyY | Y | Y | ✓ | Y | Y | ✓ |
| AgAuGdY | Y | Y | ✓ | Y | Y | ✓ |
| AgAuScY | Y | N | ✗ | Y | N | ✗ |
| AgCuScY | Y | Y | ✓ | Y | N | ✗ |
| AgPdDyGd | N | N | ✗ | N | N | ✗ |
| AgPdDyY | N* | N | ✗ | N* | N | ✗ |
| AgPdGdY | N | N | ✗ | N* | N | ✗ |
| AgPdScY | Y | Y | ✓ | Y | N | ✗ |
| AuPdScY | N* | Y | ✗ | N* | Y | ✗ |
| CuPdScY | Y | Y | ✓ | Y | N | ✗ |
| AlHfNbTi | N | Y | ✗ | N | Y | ✗ |
| AlHfTaTi | N | N | ✗ | N | Y | ✗ |
| AlMoNbTi | Y | Y | ✓ | Y | N | ✗ |
| AlNbTiV | N | N | ✗ | N | N | ✗ |

| | |
|-----------------------------------|---|
| experimentally brittle | ✗ |
| experimentally marginally ductile | ✗ |
| experimentally ductile | ✓ |
| computationally predicted brittle | ✗ |
| computationally predicted ductile | ✓ |

FIG. 6. Summary of experimental results and computational predictions for the quaternary $B2$ -like alloys with both PBE and PBEsol. Y means that the alloy fulfilled that condition while N means that the alloy failed that condition. The N* designation indicates alloys that fall within the range of the possible alteration of the necessary conditions of the metric, discussed in the text.

whether the APBs are bistable, which is required for multiple slip to occur, only λ is needed. Therefore, as a simplified application of Sun and Johnson's metric, λ is the only quantity computed in order to evaluate the sufficient condition to predict ductility. The ductility metric only considers the position of λ —either within or outside of the shaded region—so the overall magnitude of λ does not reflect the degree of ductility of an alloy. However, for all of the precious metal-rare earth alloys and two of the four refractory alloys, $\{1\bar{1}0\}$ slip is found to be dominant over $\{11\bar{2}\}$, as generally expected for bcc and $B2$ systems [5].

In the binary alloys, none of the discrepancies between the use of the PBE and PBEsol functional approximations result in changes to predictions of ductility, but based on the inconsistency with which PBEsol affects the components comprising the metric (particularly c_{44}), the quaternary alloys have been evaluated using both PBE and PBEsol. The

incorporation of the PBE and PBEsol functional approximations with the metric produce notably different results for the quaternary alloys (Fig. 6). With PBE, the metric mischaracterizes four alloys (AgCuScY, AgPdScY, CuPdScY, AlMoNbTi) while with PBEsol the metric correctly predicts the ductility of all 15 precious metal-rare earth and refractory quaternary alloys. All four of the alloys incorrectly predicted by PBE are experimentally brittle but computationally predicted ductile.

The fact that the PBEsol approximation shifts four alloys into the brittle range is not surprising, as PBEsol can be thought of as having a “tightening” effect [29]: shrinking lattice constants and increasing cohesive energies. Without further study, it is unclear whether this shift in predicted quaternary alloy ductility implies less dependence on binary cohesion energies within the quaternary alloys, but it is known that PBEsol generally sacrifices accurate cohesive (and therefore) surface energies in favor of improved lattice constants and moduli for solid systems [29]. An analysis of the inter-layer pair correlations across the faults [30] or a full cluster expansion treatment [31] could expose more clearly the dependence of the planar fault energies on binary interactions between components in the binary and quaternary alloys, though this is beyond the scope of the current study.

As shown in Fig. 5(b), several alloys are close to the upper boundary of the sufficient condition region. Each of the fault energies for every quaternary alloy have been adjusted by small amounts to test whether slight changes in these energies can make the overall ductility predictions change. This sensitivity analysis reveals that with the PBE approximation one alloy (AgAuDyGd) could change prediction from ductile to (incorrectly) brittle. With the PBEsol approximation, three alloys (AgAuScY, AgCuScY, CuPdScY) could change predictions from brittle to (incorrectly) ductile. This analysis shows that although the binarized designation of borderline cases is sensitive to relatively small changes in the fault energies, the metric with PBEsol predicts more accurately than with PBE for these quaternary alloys.

Sun and Johnson suggest using the Zener anisotropy ratio to screen candidate systems for ductility, as ductile alloys are nearly isotropic [13]. This ratio is defined as $A = c_{44}/c'$, where $c' = (c_{11} - c_{12})/2$ is the tetragonal shear modulus. To further compare the *B2*-like quaternary alloys with the systems examined by Sun and Johnson, the Zener anisotropy ratio has been calculated for the quaternary alloys with the PBEsol functional approximation; c_{44} was calculated as previously described while c' was determined by applying volume-conserving orthorhombic deformations to the unit cell, then fitting to a known energy-volume relationship following Zardach *et al.* [24]. For all of the precious metal-rare earth quaternary alloys, A is close to 1, with a range of 1.2 to 1.8, indicating that they are reasonably close to isotropic and are therefore candidates for ductility. The refractory alloys (all brittle) have larger values, with a range of 2.7 to 14.7, which is consistent with Sun and Johnson’s statement that elastically anisotropic alloys tend to lack ductility.

Some quaternary alloys studied here include species with magnetic moments such as Gd, and some binary *B2* alloys are similarly composed of magnetic species such as Ni and Fe. Although magnetism does have an effect on the lattice parameter and bonding character in *B2* and *B2*-like alloys

containing these elements, spin-polarized calculations were not performed. A motivation for developing this computational ductility metric is to screen potential alloys for experimental development, and requiring experimental classification of magnetism prior to computational evaluation with the metric is not in line with this goal. However, it would be possible to consider the effect of magnetism on the ductility metric by performing spin-polarized calculations with assumed magnetic behavior.

While binary *B2* alloys have a fixed structure, *B2*-like quaternary alloys can take on a variety of atomic configurations. Even with the assumption that size considerations will keep pairs of elements separated on sublattices, several different ordering variants are possible in quaternary Heusler-structured derivatives, including fully ordered (as used in this work), alternating columns or planes, disordered on one sublattice, and disordered on both sublattices [32]. X-ray diffraction has demonstrated that the precious metal-rare earth quaternary alloys in this study do exhibit varying levels of disorder [4]. However, because increasing atomic site disorder is thought to increase ductility [33,34], a ductility metric utilizing fully ordered *B2*-like structures should yield a conservative identification of alloys with potential for ductility. Similarly, a metric implemented with structures that include disorder on both of the quaternary sublattices should produce an optimistic estimate of ductility. A method that incorporates disorder would additionally allow for the metric to be extended to higher-order multicomponent systems that do not have ordered variants. However, indiscriminately applying this disordered approach to screen potential alloys that, if physically produced, would have ordered structures may overestimate the ductility of alloys.

An adaptation of this metric could be developed to incorporate both a conservative prediction of ductility using fully ordered structures and an optimistic prediction using disordered structures. This would require both the consideration of the necessary and sufficient condition boundaries and calculations of new structure parameters and energies. There is evidence that it would be appropriate to maintain the same condition boundaries for study of disordered bcc structures: A recent DFT study of the bcc refractory MoNbTaW showed that while the degree of short range order affects fault energies and therefore is expected to influence mechanical properties, the average equilibrium energy of a screw dislocation is not significantly affected by the degree of short range order [35]. It would then be reasonable to assume that the value of the dislocation core radius, and with this the boundaries for the necessary conditions in the metric, could remain the same.

Several adjustments to the ductility metric method can be made to model disorder in the quaternary structures. The fault energies calculated from several special quasirandom structures (SQSs) [36] should be averaged to sample configurational space. The number of SQSs should be increased until the error in the ductility metric falls below some desired threshold value, which could then be lowered to increase precision. In an example test, using five SQSs for each quaternary alloy resulted in propagated standard deviations in all three of the dimensionless quantities ($\ln C$, $\ln \delta$, λ) below a threshold of 0.1. This of course requires considerably more computational effort compared to the fully ordered metric. Furthermore, a

Monte Carlo approach employing a cluster expansion could be used to more thoroughly evaluate the effect of disorder in the fault energies [31,37,38]. This technique has the ability to capture partial ordering and produce temperature dependent properties; however, given the computational cost of fitting a cluster expansion, it may be impractical for use in a screening metric. Based on the success of the ordered metric in predicting the ductility of all 15 of the quaternary alloys, this work is evidence that the ordered metric is adequate as a computationally efficient, stand-alone metric even if a given alloy is not fully ordered.

IV. CONCLUSION

A ductility metric presented by Sun and Johnson has been confirmed for 12 *B2* transition metal intermetallics and additionally applied to 10 *B2* lanthanide intermetallics. The metric yields the same results as Sun and Johnson for the transition metal alloys and produces a comparable success rate of 70% for the lanthanide alloys, with the accuracy unchanged by switching the functional approximation from PBE to PBEsol. Two of the five mischaracterized alloys are noted to be experimentally uncertain. The results of the remaining three alloys may be skewed due to neglecting their martensitic transitions from *B2* at finite temperatures and calculations being performed at absolute zero.

We have adapted the binary ductility metric for use with *B2*-like quaternary alloys and applied it to a set of single-phase precious metal-rare earth and refractory alloys that include the first known ductile equiatomic quaternary *B2*-structured alloys. Incorporating the PBEsol functional approximation increases the accuracy of the quaternary metric results over those using the PBE functional approximation. The experimentally-measured ductilities of all 15 *B2*-like single-phase quaternary alloys are correctly predicted with PBEsol.

Though the quaternary metric incorporates fully ordered structures, several of the quaternary alloys have been shown

to demonstrate degrees of disorder by x-ray diffraction. However, our fully ordered metric successfully predicts the ductility of all the quaternary alloys in the set regardless of experimentally-observed disorder. This demonstrates the potential of the metric as a computational tool to screen quaternary *B2*-like alloys for ductility. Future adaptations of the quaternary metric could accommodate higher-order systems (greater than quaternary), nonequiatomic systems, disordered or semioordered bcc systems, and magnetic variants, leading to an even more valuable alloy design and performance engineering tool for bcc or multiphase bcc plus *B2*-structured alloys.

ACKNOWLEDGMENTS

Thank you to Bailey Meyer and Kyla Scott for production and initial characterization of the new quaternary alloys and to Dr. Karen Privat at the UNSW Electron Microscope Unit and Dr. Caitlin Healy for contributions to their characterization work. Thank you to Dr. Ruoshi Sun and Prof. Duane D. Johnson for correspondence regarding their paper. We acknowledge the support of NSF Grant No. OISE-1559403, the Jude and Eileen Laspa Fellowship at Harvey Mudd College, and the Rose Hills Foundation Science and Engineering Summer Undergraduate Research Fellowship program. This material is based upon work supported by the US Department of Energy, Office of Science, Office of Advanced Scientific Computing Research, Department of Energy Computational Science Graduate Fellowship to J.L.K. under Award No. DE-FG02-97ER25308. A.P.J. acknowledges support from DOE Grant No. DE-SC0019053. This work used the Extreme Science and Engineering Discovery Environment (XSEDE), which is supported by National Science Foundation Grant No. ACI-1548562 [39]. The authors acknowledge the Texas Advanced Computing Center (TACC) at the University of Texas at Austin for providing high performance computing resources that have contributed to the research results reported within this paper.

-
- [1] K. Gschneidner Jr., A. Russell, A. Pecharsky, J. Morris, Z. Zhang, T. Lograsso, D. Hsu, C. Chester Lo, Y. Ye, A. Slager, and D. Kesse, A family of ductile intermetallic compounds, *Nat. Mater.* **2**, 587 (2003).
- [2] K. Gschneidner Jr., M. Ji, C. Wang, K. Ho, A. Russell, Y. Mudryk, A. Becker, and J. Larson, Influence of the electronic structure on the ductile behavior of *B2* CsCl-type AB intermetallics, *Acta Mater.* **57**, 5876 (2009).
- [3] V. Paidar and M. Čák, Three types of dislocation core structure in *B2* alloys, *Intermetallics* **73**, 21 (2016).
- [4] P. L. Conway, B. Meyer, K. Scott, D. M. Miskovic, L. Bassman, and K. J. Laws (unpublished).
- [5] D. Hull and D. J. Bacon, *Introduction to dislocations*, 5th ed. (Butterworth-Heinemann, Burlington, MA, 2011).
- [6] Y. Wu and W. Hu, Elastic and brittle properties of the *B2*-MgRE (RE = Sc, Y, Ce, Pr, Nd, Gd, Tb, Dy, Ho, Er) intermetallics, *Eur. Phys. J. B* **60**, 75 (2007).
- [7] K. Gschneidner Jr., Y. Mudryk, A. Becker, and J. Larson, The crystal structures of some RM and RM₂ compounds (where R = rare earth metal and M = non - rare earth metal), *Calphad* **33**, 8 (2009).
- [8] B. Silvi and A. Savin, Classification of chemical bonds based on topological analysis of electron localization functions, *Nature (London)* **371**, 683 (1994).
- [9] A. Savin, R. Nesper, S. Wengert, and T. F. Fässler, ELF: The Electron Localization Function, *Angew. Chem. Int. Ed. Engl.* **36**, 1808 (1997).
- [10] M. Yamaguchi and Y. Umakoshi, The deformation behavior of intermetallic superlattice compounds, *Prog. Mater. Sci.* **34**, 1 (1990).
- [11] Y. Sun, Stability of APB-dissociated $\langle 111 \rangle$ screw superdislocations in *B2*-ordered structures, *Acta Metall. Mater.* **43**, 3775 (1995).
- [12] I. Baker, A review of the mechanical properties of *B2* compounds, *Mater. Sci. Eng. A* **192-193**, 1 (1995).

- [13] R. Sun and D. D. Johnson, Stability maps to predict anomalous ductility in B2 materials, *Phys. Rev. B* **87**, 104107 (2013).
- [14] D. B. Miracle, M.-H. Tsai, O. N. Senkov, V. Soni, and R. Banerjee, Refractory high entropy superalloys (RSAs), *Scr. Mater.* **187**, 445 (2020).
- [15] N. Yurchenko, N. Stepanov, S. Zherebtsov, M. Tikhonovsky, and G. Salishchev, Structure and mechanical properties of B2 ordered refractory AlNbTiVZr_x (x = 0-1.5) high-entropy alloys, *Mater. Sci. Eng. A* **704**, 82 (2017).
- [16] H. Chen, A. Kauffmann, S. Seils, T. Boll, C. Liebscher, I. Harding, K. Kumar, D. Szabó, S. Schlabach, S. Kauffmann-Weiss, F. Müller, B. Gorr, H.J. Christ, and M. Heilmaier, Crystallographic ordering in a series of Al-containing refractory high entropy alloys Ta-Nb-Mo-Cr-Ti-Al, *Acta Mater.* **176**, 123 (2019).
- [17] F. G. Coury, T. Butler, K. Chaput, A. Saville, J. Copley, J. Foltz, P. Mason, K. Clarke, M. Kaufman, and A. Clarke, Phase equilibria, mechanical properties and design of quaternary refractory high entropy alloys, *Mater. Des.* **155**, 244 (2018).
- [18] K. Momma and F. Izumi, VESTA 3 for three-dimensional visualization of crystal, volumetric, and morphology data, *J. Appl. Crystallogr.* **44**, 1272 (2011).
- [19] G. Kresse, M. Marsman, and J. Furthmüller, VASP the guide (2016), https://www.vasp.at/wiki/index.php/The_VASP_Manual.
- [20] G. Kresse and D. Joubert, From ultrasoft pseudopotentials to the projector augmented-wave method, *Phys. Rev. B* **59**, 1758 (1999).
- [21] J. P. Perdew, K. Burke, and M. Ernzerhof, Generalized Gradient Approximation Made Simple, *Phys. Rev. Lett.* **77**, 3865 (1996).
- [22] J. P. Perdew, A. Ruzsinszky, G. I. Csonka, O. A. Vydrov, G. E. Scuseria, L. A. Constantin, X. Zhou, and K. Burke, Restoring the Density-Gradient Expansion for Exchange in Solids and Surfaces, *Phys. Rev. Lett.* **100**, 136406 (2008).
- [23] P. E. Blöchl, O. Jepsen, and O. K. Andersen, Improved tetrahedron method for Brillouin-zone integrations, *Phys. Rev. B* **49**, 16223 (1994).
- [24] A. J. Zaddach, C. Niu, C. C. Koch, and D. L. Irving, Mechanical properties and stacking fault energies of NiFeCrCoMn high-entropy alloy, *JOM* **65**, 1780 (2013).
- [25] M. Ibarra, T. Chien, and A. Pavlovic, Structural instability in RCu intermetallic compounds, *J. Less Common Met.* **153**, 233 (1989).
- [26] M. R. Ibarra, C. Marquina, A. S. Pavlovic, and C. Ritter, Study of the influence of the magnetoelastic energy in driving the magnetic and structural transition in TbCu, *J. Appl. Phys.* **70**, 5989 (1991).
- [27] See Supplemental Material at <http://link.aps.org/supplemental/10.1103/PhysRevMaterials.5.033604> for metric quantities, mechanical properties, and defect energies.
- [28] W. Xu and J. A. Moriarty, Atomistic simulation of point defects and dislocations in bcc transition metals from first principles, *J. Comput.-Aided Mater. Des.* **3**, 245 (1996).
- [29] G.-X. Zhang, A. M. Reilly, A. Tkatchenko, and M. Scheffler, Performance of various density-functional approximations for cohesive properties of 64 bulk solids, *New J. Phys.* **20**, 063020 (2018).
- [30] J. L. Kaufman, G. S. Pomrehn, A. Pribram-Jones, R. Mahjoub, M. Ferry, K. J. Laws, and L. Bassman, Stacking fault energies of nondilute binary alloys using special quasirandom structures, *Phys. Rev. B* **95**, 094112 (2017).
- [31] A. R. Natarajan and A. Van der Ven, Linking electronic structure calculations to generalized stacking fault energies in multicomponent alloys, *npj Comput. Mater.* **6**, 80 (2020).
- [32] P. Neibecker, M. E. Gruner, X. Xu, R. Kainuma, W. Petry, R. Pentcheva, and M. Leitner, Ordering tendencies and electronic properties in quaternary Heusler derivatives, *Phys. Rev. B* **96**, 165131 (2017).
- [33] D. G. Pettifor, Theoretical predictions of structure and related properties of intermetallics, *Mater. Sci. Technol.* **8**, 345 (1992).
- [34] T. Davies and A. Ogwu, A possible route to improving the ductility of brittle intermetallic compounds, *J. Alloys Compd.* **228**, 105 (1995).
- [35] S. Yin, J. Ding, M. Asta, and R. O. Ritchie, Ab initio modeling of the energy landscape for screw dislocations in body-centered cubic high-entropy alloys, *npj Comput. Mater.* **6**, 110 (2020).
- [36] A. Zunger, S.-H. Wei, L. G. Ferreira, and J. E. Bernard, Special Quasirandom Structures, *Phys. Rev. Lett.* **65**, 353 (1990).
- [37] R. Sun and A. van de Walle, Automating impurity-enhanced antiphase boundary energy calculations from ab initio Monte Carlo, *Calphad* **53**, 20 (2016).
- [38] R. Sun, C. Woodward, and A. van de Walle, First-principles study on Ni₃Al (111) antiphase boundary with Ti and Hf impurities, *Phys. Rev. B* **95**, 214121 (2017).
- [39] J. Towns, T. Cockerill, M. Dahan, I. Foster, K. Gaither, A. Grimshaw, V. Hazlewood, S. Lathrop, D. Lifka, G. D. Peterson, R. Roskies, J. R. Scott, and N. Wilkins-Diehr, XSEDE: Accelerating scientific discovery, *Comput. Sci. Eng.* **16**, 62 (2014).